Dopamine Receptors Influence Internally Generated Oscillations during Rule Processing in Primate Prefrontal Cortex

Torben Ott*, Stephanie Westendorff, and Andreas Nieder

Abstract

■ Neural oscillations in distinct frequency bands in the prefrontal cortex (pFC) are associated with specialized roles during cognitive control. How dopamine modulates oscillations to structure pFC functions remains unknown. We trained macaques to switch between two numerical rules and recorded local field potentials from pFC while applying dopamine receptor targeting drugs using microiontophoresis. We show that the D1 and D2 family receptors (D1Rs and D2Rs, respectively) specifically altered internally generated prefrontal oscillations, whereas sensory-evoked potentials remained unchanged. Blocking D1Rs or stimulating D2Rs increased low-frequency theta and alpha oscillations known to be involved in learning and memory. In contrast, only D1R inhibition enhanced high-frequency beta oscillations, whereas only D2R stimulation increased gamma oscillations linked to top–down and bottom–up attentional processing. These findings suggest that dopamine alters neural oscillations relevant for executive functioning through dissociable actions at the receptor level. ■

INTRODUCTION

Rules guide our decision-making in novel situations. Flexibly switching between rules based on context is a hallmark feature of executive control (Stoet & Snyder, 2009). To apply rules, information about sensory input and internal states represented in different brain areas needs to be integrated. Neural networks may overcome this challenge by synchronizing activity in neural ensembles, thereby giving rise to neural oscillations (Singer, 2009; Uhlhaas et al., 2009; Womelsdorf & Fries, 2007).

The prefrontal cortex (pFC), operating at the apex of the cortical hierarchy (Miller & Cohen, 2001), shows a distinct pattern of neural oscillations in different frequency bands during cognitive behavior (Benchenane, Tiesinga, & Battaglia, 2011). For example, theta oscillations have been suggested to be involved in learning and updating memory (Raghavachari et al., 2001), and alpha oscillations are elevated during the suppression of task-irrelevant behavior (Roux & Uhlhaas, 2014). Beta and gamma oscillations, in contrast, have been proposed to play distinct roles in attentional processing. More specifically, beta oscillations are thought to contribute to top–down attentional control (Buschman & Miller, 2007) and the maintenance of current cognitive states (Engel & Fries, 2010), whereas gamma oscillations have been hypothesized to mediate bottom–up attention contributing to behavioral flexibility (Miller & Buschman, 2013; Sohal, Zhang, Yizhar, & Deisseroth, 2009).

All of the cardinal functions of pFC, such as working memory or conceptualization, are regulated by the neuromodulator dopamine (Robbins & Arnsten, 2009; Brozoski, Brown, Rosvold, & Goldman, 1979). Dopamine acts via D1 and D2 family receptors (D1Rs and D2Rs, respectively), which distinctly contribute to executive control (Ott & Nieder, 2017; Ott, Jacob, & Nieder, 2014). Both dopamine receptor families modulate sustained working memory activity (Ott & Nieder, 2017; Ott et al., 2014; Vijayraghavan, Wang, Birnbaum, Williams, & Arnsten, 2007), but D1Rs are hypothesized to stabilize prefrontal representations, whereas D2Rs are implicated in switching between behavioral strategies to updating task-relevant prefrontal representations (Durstewitz & Seamans, 2008; Floresco, Magyar, Ghods-Sharifi, Vexelman, & Tse, 2006; Seamans & Yang, 2004).

Dopamine has been shown to modulate cortical oscillations across various frequency bands. In rodents, D2R stimulation increases gamma power in frontal cortex (Kocsis, Lee, & Deth, 2014) and hippocampus (Andersson, Johnston, & Fisahn, 2012). D1R manipulation has been shown to alter behavior-dependent delta and alpha power (Parker, Ruggiero, & Narayanan, 2015; Parker, Chen, Kingyon, Cavanagh, & Narayanan, 2014). In monkeys, blocking prefrontal D1Rs broadly increases alpha and beta power related to novel associations (Puig, Rose, Schmidt, & Freund, 2014), whereas the effect of blocking D2Rs is constricted to increasing narrow band alpha power (Puig & Miller, 2015).

University of Tübingen
*Present address: Cold Spring Harbor Laboratory, 1 Bungtown Road, Cold Spring Harbor, NY 11724, USA.

doi:10.1162/jocn_a_01248

However, it is unknown how dopamine receptors modulate pFC oscillations during rule-guided processes. Here we hypothesized that D1Rs and D2Rs play distinct roles in modulating neural oscillations in pFC that are associated with different cognitive functions. Specifically, the proposed functional role for D1Rs in stabilizing cognitive states predicts a specific D1R modulation of beta oscillations as reported earlier (Puig et al., 2014). On the other hand, D2Rs may modulate gamma oscillations as found in rodents (Kocsis et al., 2014; Andersson et al., 2012), because D2Rs are thought to mediate updating of pFC representations. Such mechanisms for updating prefrontal representations might entail either the direct modulation of externally driven ERPs (Brincat & Miller, 2016) or, alternatively, of internally driven neural oscillations such as theta oscillations; the latter have been implicated in gating STM.

To test these hypotheses, we analyzed oscillatory signatures of local field potentials (LFPs) while iontophoretically applying dopamine receptor targeting drugs in monkeys performing a numerical rule-switching task (Ott & Nieder, 2017; Nieder, 2016; Ott et al., 2014). We show that dopamine receptors modulate LFP power indicative for ongoing neural oscillations in pFC during rule-guided decisions through dissociable mechanisms at the receptor level.

METHODS

Animals and Surgical Procedures

Two male rhesus monkeys (*Macaca mulatta*) were implanted with a titanium head post and one recording chamber centered over the principal sulcus of the lateral pFC, anterior to the FEFs (right hemispheres in both monkeys). Surgery was conducted using aseptic techniques under general anesthesia. Structural magnetic resonance imaging was performed before implantation to locate anatomical landmarks. All experimental procedures were in accordance with the guidelines for animal experimentation approved by the authority, the Regierungspräsidium Tübingen, Germany.

Task

Monkeys learned to flexibly perform numerical "greater than" versus "less than" comparisons. They initiated a trial by grasping a lever and maintaining central fixation on a screen. After a pure fixation period (500 msec), a sample stimulus (500 msec) cued the animals for the reference numerosity (i.e., number of dots) they had to remember for a brief time interval. The first memory interval (Delay 1, 1000 msec) was followed by a rule cue (300 msec) that instructed the monkeys to select either a larger number of dots ("greater than" rule, red circle or white circle with water) or a smaller number of dots ("less than" rule, blue circle or white circle with no water) than the sample numerosity in the subsequent test phase. The test phase was preceded by a second delay (Delay 2, 1000 msec) requiring the monkeys to assess the rule at hand for the subsequent choice. In the following Test 1 phase, the monkeys had to release the lever in a "greater than" trial, if the number of items in the test display was larger than the number of items in the sample display (match trial), or to keep holding the lever for another 1200 msec until the appearance of a second test display (Test 2), if the number of items in the test display was smaller than the number of items in the sample display (nonmatch trial). In a "less than" trial, these conditions were reversed. Monkeys got a liquid reward for a correct choice. Thus, only Test 1 required a decision; Test 2 was used so that a behavioral response was required in each trial, ensuring that the monkeys were paying attention during all trials. Because both sample and test numerosities varied randomly, the monkeys could only solve the task by assessing the numerosity of the test display relative to the three possible numerosities of the sample display together with the appropriate rule in any single trial. To test a range of numerosities, both monkeys were presented with numerosities 2 (smaller test numerosity = 1, larger test numerosity = 4), 8 (4:16), and 32 (16:64). For any sample numerosity, test numerosities were either larger or smaller with equal probability ($p = .5$). Because the monkeys' numerosity discrimination performance obeys the Weber–Fechner law (Nieder & Miller, 2003), numerosities larger than a sample numerosity need to be numerically more distant than numerosities smaller than the sample numerosity to reach equal discriminability. Based on this design, any test numerosity (except the smallest and largest used) served as test numerosities for different sample numerosities, thus precluding the animals from learning systematic relations between numerosities.

To prevent the animals from exploiting low-level visual cues (e.g., dot density, total dot area), a standard numerosity protocol (with dot sizes and positions pseudorandomized) and a control numerosity protocol (with equal total area and average density of all dots within a trial) were each presented in 50% of the trials in a pseudorandomized fashion. To dissociate the rule-related cellular responses from responses to the sensory features of the rule cue, each rule was signified by two different rule cues in two different sensory modalities: a red circle ("greater than" rule, red color) or a white circle with a drop of water ("greater than" rule, water) signified the rule "greater than." The "less than" rule was cued by a blue circle ("less than" rule, blue color) or a white circle with no water ("less than" rule, no water). We showed in previous studies that monkeys generalize the numerical principles "greater than" and "less than" to numerosities they had never seen before (Eiselt & Nieder, 2013; Bongard & Nieder, 2010). Before each session, the displays were generated anew using MATLAB (The MathWorks, Natick, MA). Trials were randomized and balanced across all

relevant features ("greater than" and "less than" rules, rule cue modalities, sample numerosities, standard and control stimuli, and match and nonmatch trials). Monkeys had to keep their gaze within 1.75° of the fixation point from the fixation interval up to the onset of the first test stimulus (monitored with an infrared eye-tracking system; ISCAN, Burlington, MA).

Electrophysiology and Iontophoresis

Extracellular single-unit recording and iontophoretic drug application was performed as described previously (Ott & Nieder, 2017; Ott et al., 2014; Jacob, Ott, & Nieder, 2013). In each recording session, up to three custom-made tungsten-in-glass electrodes flanked by two pipettes each were inserted transdurally using a modified electrical microdrive (NAN Instruments). The site of recording of single-unit activity and LFPs was chosen at random; no attempt was made to preselect the neurons or LFPs to any task-related activity or based on drug effects. Signal acquisition, amplification, filtering, and digitalization were accomplished with the MAP system (Plexon). For LFPs, voltage signals were preamplified (gain 1000), bandpass filtered from 0.7 to 300 Hz, and digitized with 1000 Hz. Drugs were applied iontophoretically (MVCS iontophoresis system; npi electronic) using custom-made tungsten-in-glass electrodes flanked by two pipettes each (Ott & Nieder, 2017; Ott et al., 2014; Jacob et al., 2013; Thiele, Delicato, Roberts, & Gieselmann, 2006). Electrode impedance and pipette resistance were measured after each recording session. Electrode impedances were 0.8–3 MΩ (measured at 500 Hz; Omega Tip Z; World Precision Instruments). Pipette resistances depended on the pipette opening diameter, drug, and solvent used. Typical resistances were 15–50 MΩ (full range, 12–160 MΩ). As in previous experiments (Ott & Nieder, 2017; Ott et al., 2014; Jacob et al., 2013), we used retention currents of −7 nA to hold the drugs in the pipette during control conditions. The ejection current for SKF81297 (10 mM in double-distilled water, pH 4.0 with HCl; Sigma-Aldrich) was +15 nA, the ejection current for SCH23390 (10 mM in double-distilled water, pH 4.0 with HCl; Sigma-Aldrich) was +25 nA, and the ejection current for quinpirole (10 mM in double-distilled water, pH 4.0 with HCl; Sigma-Aldrich) was +40 nA. In control experiments with 0.9% physiological NaCl, pH 4.0 with HCl, the ejection current was +25 nA. We did not investigate dosage effects and chose ejection currents to match the values reported to be maximally effective, that is, in the peak range of the "inverted-U function" (Vijayraghavan et al., 2007; Wang, Vijayraghavan, & Goldman-Rakic, 2004). One pipette per electrode was filled with drug solution (either SKF81297, SCH23390, quinpirole, or NaCl), and the other always contained 0.9% NaCl. In each recording session, control conditions using the retention current alternated with drug conditions using the ejection current. Drugs were applied continuously for 12–15 min (drug conditions), depending on the number of trials completed correctly by the animal. Each control or drug application block consisted of 72 correct trials to yield sufficient trials for analysis. The first block (12–15 min) was always the control condition. Given that iontophoretic drug application is fast and can quickly modulate neuronal firing properties (Jacob et al., 2013), we did not exclude data at the current switching points. LFP recordings in both monkeys were made using the same recording chamber, that is, in the same overall anatomical locations, across all experiments. We observed slight channel-to-channel variations in LFP power, which likely stem from small variations in recording depth and electrode placement during acute recordings. All drug-induced changes in LFP power were analyzed as paired statistics over channels, thus taking into account potential differences between channels.

Data Analyses

Preprocessing and power extraction of LFP time series was performed using MATLAB and the fieldtrip toolbox. For evoked potentials, raw LFP traces were averaged time-locked to the onset of the sample stimulus. To avoid biases in baseline power due to different number of trials in the average, which could arise if more trials contribute to the average cancelling out LFP fluctuations, we equalized the number of trials for control and drug conditions by randomly drawing trials (without replacement) according to the lower number of trials for each channel. To quantify internally generated LFP power not phase-locked to external task events, we subtracted evoked potentials from raw LFP traces of each trial separately for control and drug conditions. For both evoked and internally generated potentials, we removed line noise at 50, 100, and 150 Hz using the discrete Fourier transform. LFP power was extracted with multitaper time–frequency transformation based on multiplication in the frequency domain using Hanning tapers. We defined frequencies of interest between 4 and 40 Hz using steps of 1.5 Hz and between 40 and 60 Hz using steps of 4.5 Hz. The length of the time window for each frequency was four times the corresponding cycle length. To calculate intertrial coherence (ITC), we averaged the phase angle of the LFP in each frequency and time bin over trials computed from the single trial Fourier spectra. We did not investigate LFP power above 60 Hz because spike intrusions can confound LFP signals (Ray & Maunsell, 2011).

Only channels with at least 25 trials were used, and channels with obvious artifacts visible in their power spectra were excluded (n = 6 channels). The remaining 308 channels entered subsequent analyses. Trials in which the LFP signal was close to saturation were excluded from analyses (absolute signal larger than 250 μV). For power spectra analyses, we computed the average power using the time bins that fell within the period of interest. We then calculated trial averages and report statistics over the channels. For time series analyses, we

calculated the baseline power for each trial by first averaging time bins within 0–300 msec from fixation onset. We then calculated, for each channel, the mean and the standard deviation of baseline power over trials. We used condition-averaged normalization combining control and drug trials. We then z-scored time series by subtracting the mean baseline from the trial-averaged power of each time and frequency bin and dividing by the standard deviation of the baseline, separate for control and drug conditions. For time–frequency plots, we slightly smoothed the LFP power using a 2-D Gaussian kernel with standard deviation of 1.5 windows (75 msec) in the time axis and standard deviation of 0.5 windows (0.75 Hz) in the frequency axis.

For rule-specific LFP signals, we separated trial-averaged LFP power for trials in which the "greater than" rule was in effect and trials in which the "less than" rule was in effect. For calculating power spectra, we used the last 800 msec of the Delay 2 period, that is, beginning 200 msec after rule cue offset. Single-unit activity shows strongest rule selectivity during the time period (Ott et al., 2014). We calculated a rule modulation index, quantifying the LFP dependency on the numerical rule for a given time period and frequency band. We defined two frequency bands based on the observed significant dependence of LFP power on the numerical rules: A "beta" band ranging from 24 to 36 Hz and a "gamma" band ranging from 46 to 60 Hz. Power was averaged during the same time period in the Delay 2 period, over the frequency bin in the respective power band, and over trials. We then calculated, for each channel, a rule modulation index by subtracting the average power of "less than" from "greater then" trials and dividing by the sum, separate for control and drug conditions. We repeated this analyses for a subset of channels, for which we observed a significant drug-induced power modulation in either the beta or gamma band (defined as above) using a rank sum test ($p < .05$).

RESULTS

We trained two macaque monkeys in a delayed response task to switch between the numerical rules "greater than" and "less than" (Figure 1A). Both monkeys learned to proficiently apply the rules showing high performance for different sample numerosities ("2," "8," "32"), both

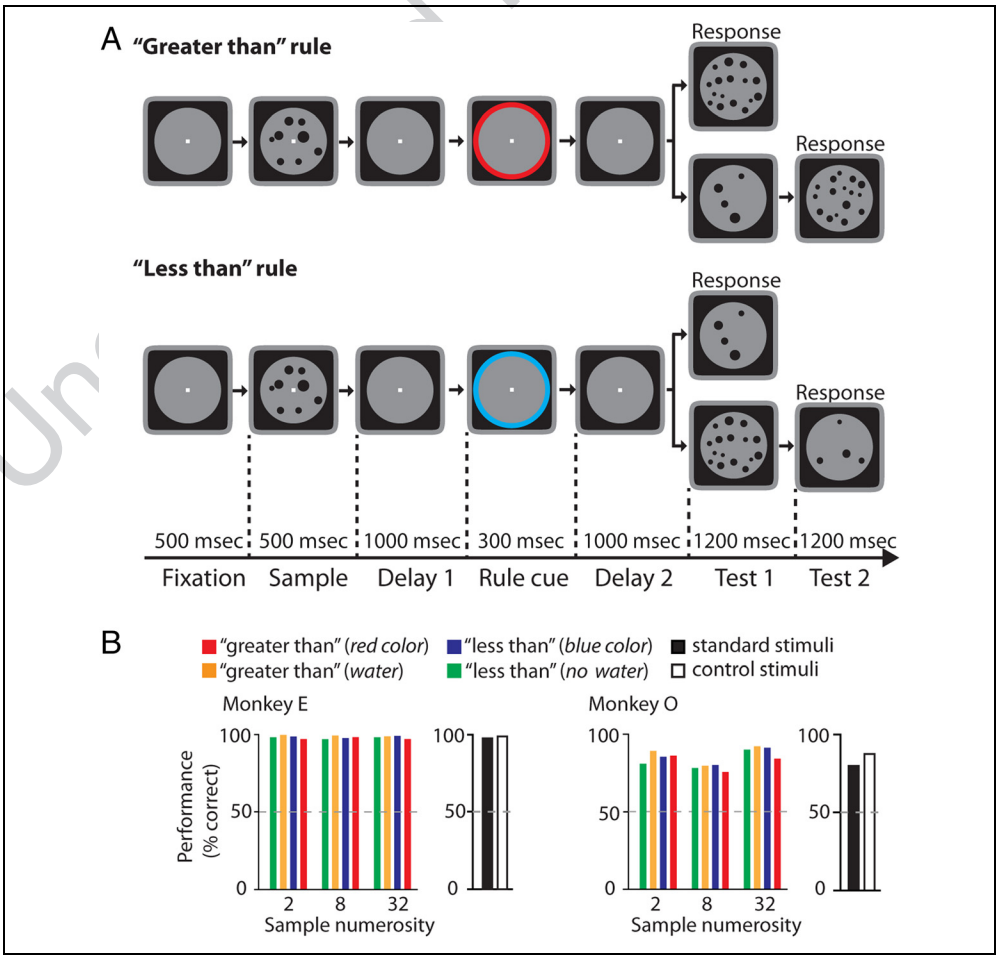

Figure 1. Numerical rule-switching task and behavioral performance. (A) Task protocol. The monkeys compared the numbers of dots in a display (numerosities) by applying the numerical rules "greater than" or "less than." The "greater than" rule required the monkeys to release a lever (response) if the first test display showed more dots than the sample display, whereas the "less than" rule required a lever release if the number of items in the first test display was smaller compared with the sample display. For each trial, the rule to apply ("greater than" vs. "less than") was indicated by a cue that was presented in the delay between sample and test stimuli. (B) Performance (% correct trials) of the two monkeys for each sample numerosity and for each rule cue. Two distinct set of rule cues were used: a color cue set (depicted in A) and a gustatory cue set with same visual appearance using a water cue ("greater than") or no water ("less than"). Performance was equal in trials with standard stimuli (black) and control trials (white) using stimuli with equal dot area and density (see Methods). Dotted line indicates chance performance (50%).

numerical rules ("greater than," "less than"), both rule cue sets (blue/red, water/no water), and both stimulus sets (standard set with random dot displays, control set with equal density and surface area of dot displays; Figure 1B).

We implanted recording chambers above the principal sulcus of both monkeys allowing for acute recordings of single-unit activity and LFPs in pFC and simultaneous iontophoretic drug application using electrode–pipette combinations. In each recording session, we alternated between control conditions without drug application and drug conditions with continuous drug ejection of dopamine receptor targeting drugs using either the D1R agonist SKF81297 (87 channels), the D1R antagonist SCH23390 (97 channels), the D2R agonist quinpirole (67 channels), or normal saline as a control (57 channels). We reported dopamine receptor effects on single-unit activity previously (Ott & Nieder, 2017; Ott et al., 2014). Here we focused on drug-induced effects on neural oscillations measured by LFPs.

We investigated whether dopamine either affects LFP power driven by external stimulation (i.e., bottom–up) or ongoing oscillations internally generated by the neural network based on cognitive processes such as working memory or rule application (i.e., top–down; Brincat & Miller, 2016). Because we find that dopamine receptors did not modulate purely sensory-evoked potentials to external visual stimuli, the main part of the study deals with internally generated oscillations.

Dopamine Receptors Do Not Modulate Evoked Potentials to External Stimuli

First, we assessed if dopamine receptor stimulation modulated evoked LFPs to external stimuli. To that aim, we averaged raw LFP traces triggered to the onset of the sample stimulus the monkeys had to memorize and then analyzed LFP power. That way, LFP power reflects evoked potentials driven by the visual stimuli and is therefore considered externally driven. We found sensory-evoked sharp increases in low-frequency theta and alpha band power (4–20 Hz) following visual stimulation (Figure 2). Notably, however, dopamine receptor modulation did not modulate these evoked potentials. Stimulating or blocking D1Rs (with SKF81297 or SCH23390, respectively) did not lead to any changes in evoked potentials to the sample stimulus or to the rule cue ($p > .01$ in any frequency band comparing control and drug conditions, signed rank test; Figure 2A–F). Similarly, stimulating D2Rs (with quinpirole) did not change evoked potentials in either task phase (Figure 2G–I). Control experiments with saline also did not lead to any changes in evoked LFPs (Figure 2J–L). In addition, we computed the ITC to assess potential phase-locking of LFP power to the time of the stimulus, which could serve as evidence for a phase reset of neural oscillations (Sauseng et al., 2007). Time-dependent ITCs showed sharp peaks following stimulus presentation in low-frequency bands reflecting the trial-averaged power spectrum. We did not find any ITC peaks distinct from the trial-averaged power spectrum; thus, no evidence for phase reset of potential ongoing oscillations. Applying dopamine receptor targeting drugs did not alter ITCs in any frequency band (Figure 3). Thus, dopamine receptors do not modulate purely sensory-evoked potentials to external visual cues in pFC.

Dopamine Receptors Differentially Modulate Baseline LFP Power

Next, we assessed how dopamine receptor stimulation modulated LFP power potentially underlying internally generated oscillations. For each channel, we subtracted trial-averaged LFPs from the raw LFP traces of each trial. Subsequently, we extracted LFP power using the Fourier transforms for each trial and averaged the power over trials. Remaining LFP powers thus only include power components that are not phase-locked to external sensory stimuli. First, we asked whether dopamine receptors modulate baseline LFPs during the pure fixation period (i.e., the first 300 msec of a trial).

Influencing D1Rs changed baseline LFP power relative to the control condition without drug application. Stimulation of D1Rs (with SKF81297) lead to an increase in LFP power in the beta range from 25 to 32 Hz (ΔPower = $+6.1 \pm 3.0\ \mu V^2$, $n = 87$, signed rank test, $p < .01$ in six consecutive frequency bands; Figure 4A). In contrast, blocking D1Rs (using SCH23390) increased the low-frequency theta/alpha power between 4 and 15 Hz (ΔPower = $3.9 \pm 0.8\ \mu V^2$, $n = 97$, $p < .01$ in eight consecutive frequency bands; Figure 4B). In addition, blocking D1Rs increased power in the low gamma range between 32 and 42 Hz (ΔPower = $5.6 \pm 1.8\ \mu V^2$, $n = 97$, $p < .01$ in five consecutive frequency bands; Figure 4B). This low gamma band affected by D1Rs inhibition was distinct from the beta band that was influenced by D1Rs stimulation.

Stimulating D2Rs (with quinpirole) also increased LFP power in the alpha range between 7 and 19 Hz (ΔPower = $6.1 \pm 2.0\ \mu V^2$, $n = 67$, $p < .01$ in nine consecutive frequency bands; Figure 4C). However, in contrast to D1R-induced modulation, D2R stimulation increased LFP power in the high-frequency gamma range between 46 and 60 Hz (ΔPower = $4.4 \pm 1.1\ \mu V^2$, $n = 67$, $p < .01$ in four consecutive frequency bands; Figure 4C).

All observed LFP changes were drug-induced. When we applied normal saline as a control, no LFP power modulation in any frequency band was observed ($n = 57$, $p > .01$, any bin; Figure 4D). In summary, D1Rs and D2Rs influenced LFP power in distinct frequency bands: Both blocking D1Rs and stimulating D2Rs increased low-frequency theta/alpha band power. Beta/low gamma band power was enhanced by blocking D1Rs only, whereas an increase of gamma band power was only observed after stimulating D2Rs.

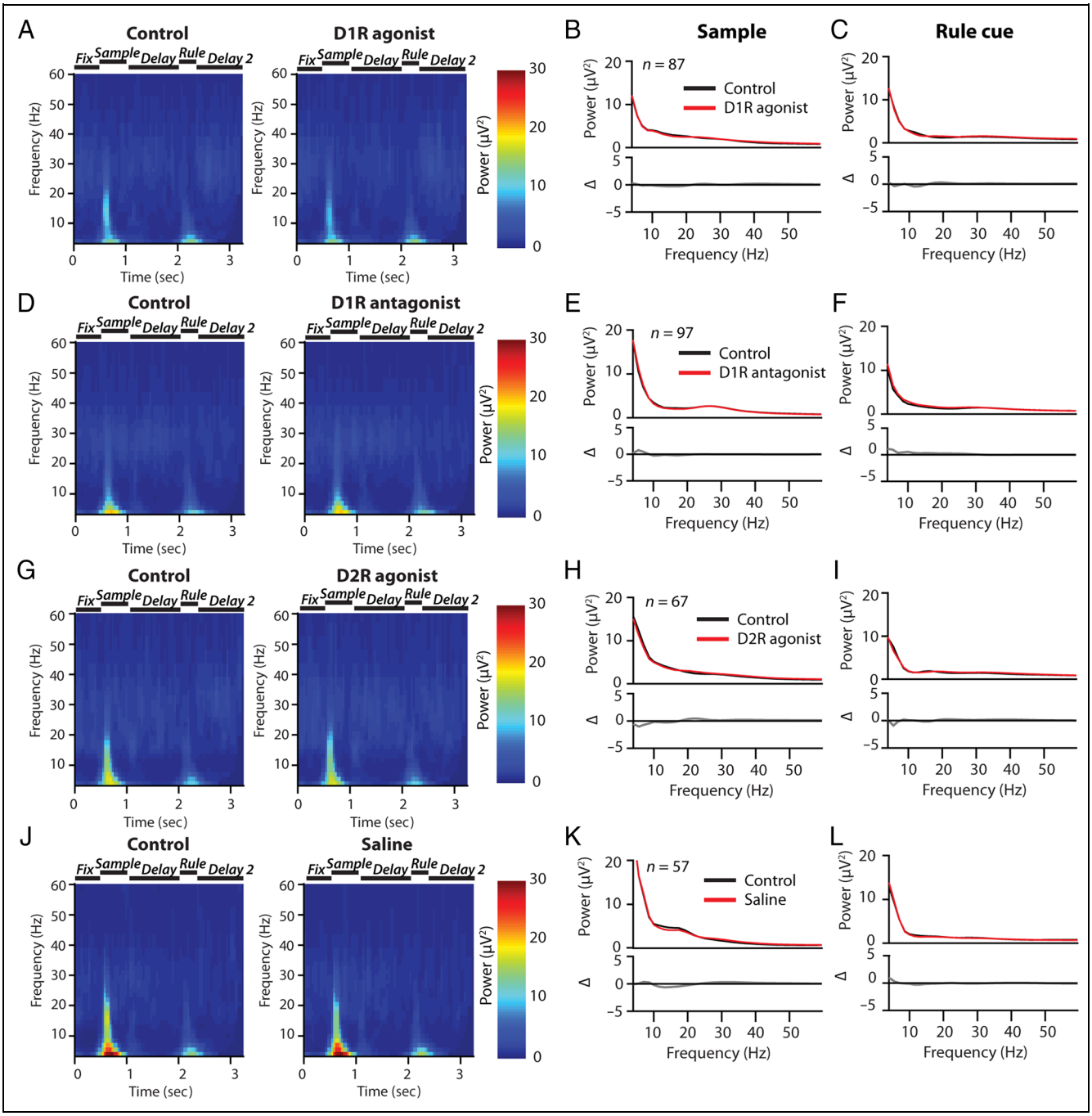

Figure 2. Dopamine receptors did not modulate sensory-evoked potentials. (A) Time–frequency plot showing externally driven neural oscillations with color-coded LFP power for control conditions (left) and after SKF81297 (D1R agonist) application (middle) and the difference between drug and control (right). (B) Trial-averaged sensory-evoked potentials during the stimulus period (500 msec period starting 100 msec after sample presentation) for control conditions and during stimulating D1Rs (top). Scaled up difference between drug and control (bottom) did not reveal any LFP modulation. (C) Conventions as in B for the rule cue period (300 msec starting 100 msec after rule cue presentation) for SKF81297. (D) Same conventions as in A for D1R blockade with SCH23390. (E) Same conventions as in B for SCH23390. (F) Same conventions as in C for SCH23390. (G) Same conventions as in A for stimulating D2Rs with quinpirole. (H) Same conventions as in B for quinpirole. (I) Same conventions as in C for quinpirole. (J) Same conventions as in A for saline controls. (K) Same conventions as in B for saline controls. (L) Same conventions as in C for saline controls. Gray line denotes nonsignificant differences between drug and control conditions ($p > .01$ in each frequency bin, signed rank test).

Time-dependent Modulation of LFP Power

Next, we assessed the time course of LFP power during the delay period of the numerical rule task. We normalized LFP power to baseline using z-scores (i.e., we subtracted baseline power and divided by baseline power's standard deviation). For illustrative purposes, we draw heat maps of LFP power across frequencies during the course

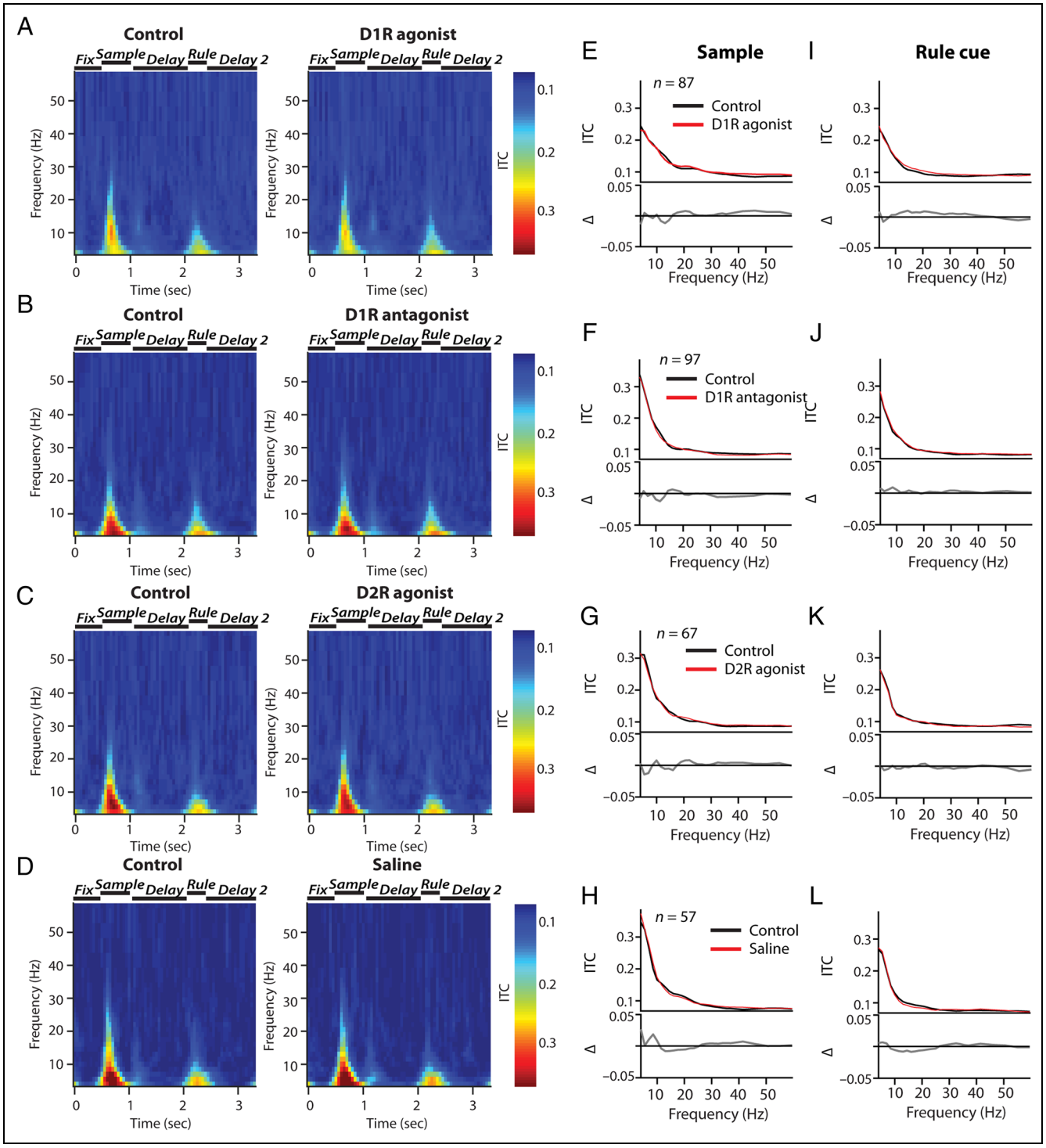

Figure 3. Dopamine receptors did not modulate ITC. (A) Time–frequency plot showing stimulus-locked phase coherence with color-coded ITC for control conditions (left) and after SKF81297 application (right). (B) Trial-averaged ITCs during the stimulus period (500 msec period starting 100 msec after sample presentation) for control conditions and after stimulating D1Rs (top). Scaled up difference between drug and control (bottom) did not reveal any ITC modulation. (C) Conventions as in B for the rule cue period (300 msec starting 100 msec after rule cue presentation) for SKF81297. (D) Same conventions as in A for D1R blockade with SCH23390. (E) Same conventions as in B for SCH23390. (F) Same conventions as in C for SCH23390. (G) Same conventions as in A for stimulating D2Rs with quinpirole. (H) Same conventions as in B for quinpirole. (I) Same conventions as in C for quinpirole. (J) Same conventions as in A for saline controls. (K) Same conventions as in B for saline controls. (L) Same conventions as in C for saline controls. Gray line denotes nonsignificant differences between drug and control conditions ($p > .01$ in each frequency bin, signed rank test).

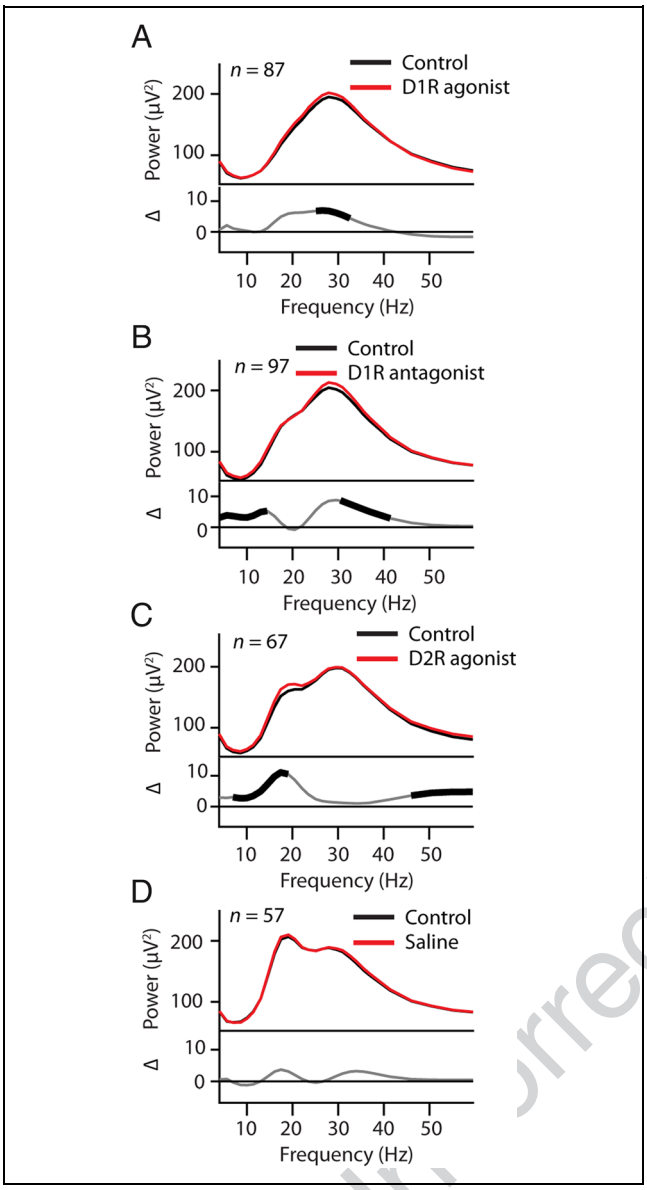

Figure 4. Dopamine receptors differentially modulated internally generated LFPs. (A) Trial-averaged internally generated LFP power spectra for control conditions and after stimulating D1Rs using SKF81297 (top) in the baseline period (pure fixation). Scaled up difference between drug and control (bottom) shows an increase in LFP power between 24 and 31 Hz after D1R stimulation (marked by thick line segment in the bottom plot). (B) Same conventions as in A for blocking D1Rs using SCH23390 showing an increase in LFP power between 4 and 14 Hz and between 30 and 42 Hz. (C) Same conventions as in A) for D2R stimulation using quinpirole showing an increase in LFP power between 7 and 19 Hz and above 46 Hz. (D) Same conventions as in A for saline control with no modulation of LFP power. *N*, number of channels; thick lines correspond to frequencies with significant drug-induced changes in LFP power ($p < .01$, signed rank test).

of the trial (Figure 5). After visual cues (i.e., presentation of sample numerosity and rule cue), phasic peaks in the theta/alpha range (5–15 Hz) occurred in control and drug conditions. These were followed by a persistent decrease in power in the beta/low gamma range around 30 Hz during delay periods, which peaked during baseline (Figure 4). Some channels also showed an increase in power in the beta/low gamma range during delay periods. These task-dependent peaks in LFP power are indicative of rhythmic brain activity and thus provide evidence that LFP power in the different frequency bands reflect ongoing neural oscillations (Lopes da Silva, 2013; Siegel, Donner, Oostenveld, Fries, & Engel, 2008).

D1R stimulation did not result in prominent changes of LFP patterns during the trial (Figure 5A). In contrast, blocking D1Rs showed a noticeable increase of LFP power in the alpha range around 10 Hz. This effect was particularly strong during phasic rises of theta/alpha power after sample presentation and before and around the presentation of the rule cue (Figure 5B). Beta/low gamma power around 30 Hz was also increased by D1R blockade. For D2R stimulation, we also observed an increase in low-frequency theta/alpha power, as well as an increase in high gamma power above 45 Hz (Figure 5C). Application of normal saline did not produce changes in LFP power during the trial (Figure 5D). This confirms drug-induced effects on LFP power during the course of the trial.

LFP Power Is Rule-dependent

Next, we examined internally generated oscillations during the cognitively most demanding time period, the Delay 2 period in which the abstract numerical rule needed to be represented for the monkey to choose the right test numerosity. To that aim, we calculated raw LFP power during the Delay 2 period for correct trials in which the "greater than" rule was cued and for correct trials in which the "less than" rule was cued. This was done by pooling control conditions from all channels.

We found that the intensity of LFP power in different frequency bands was dependent on the numerical rule: For "less than" rule trials, LFP power was higher compared with "larger than" rule trials in the beta/low gamma range between 23 and 36 Hz ($\Delta\text{Power} = -4.7 \pm 1.2\ \mu V^2$, $n = 308$, $p < .01$ in nine consecutive frequency bands; Figure 6A). In contrast, LFP power in the high gamma range between 46 and 60 Hz was higher for "larger than" trials compared with "less than" trials ($\Delta\text{Power} = +4.2 \pm 0.8\ \mu V^2$, $n = 308$, $p < .01$ in four consecutive frequency bands; Figure 6A). These differences were observed throughout the time course of the Delay 2 period and were most prominent at the end of the delay period before the choice (Figure 6B). During the Delay 2 period, we observed LFP power peaks in the alpha and gamma range and power troughs in the beta range (Figure 6B), which showed a peak during the baseline (Figure 4A), indicative of ongoing neural oscillations.

Strikingly, LFP power in the two rule-specific frequency bands (beta and high gamma) were differentially modulated by dopamine receptor families during the Delay 2 period. Although stimulating D1Rs did not show obvious LFP power modulation during the Delay 2 period

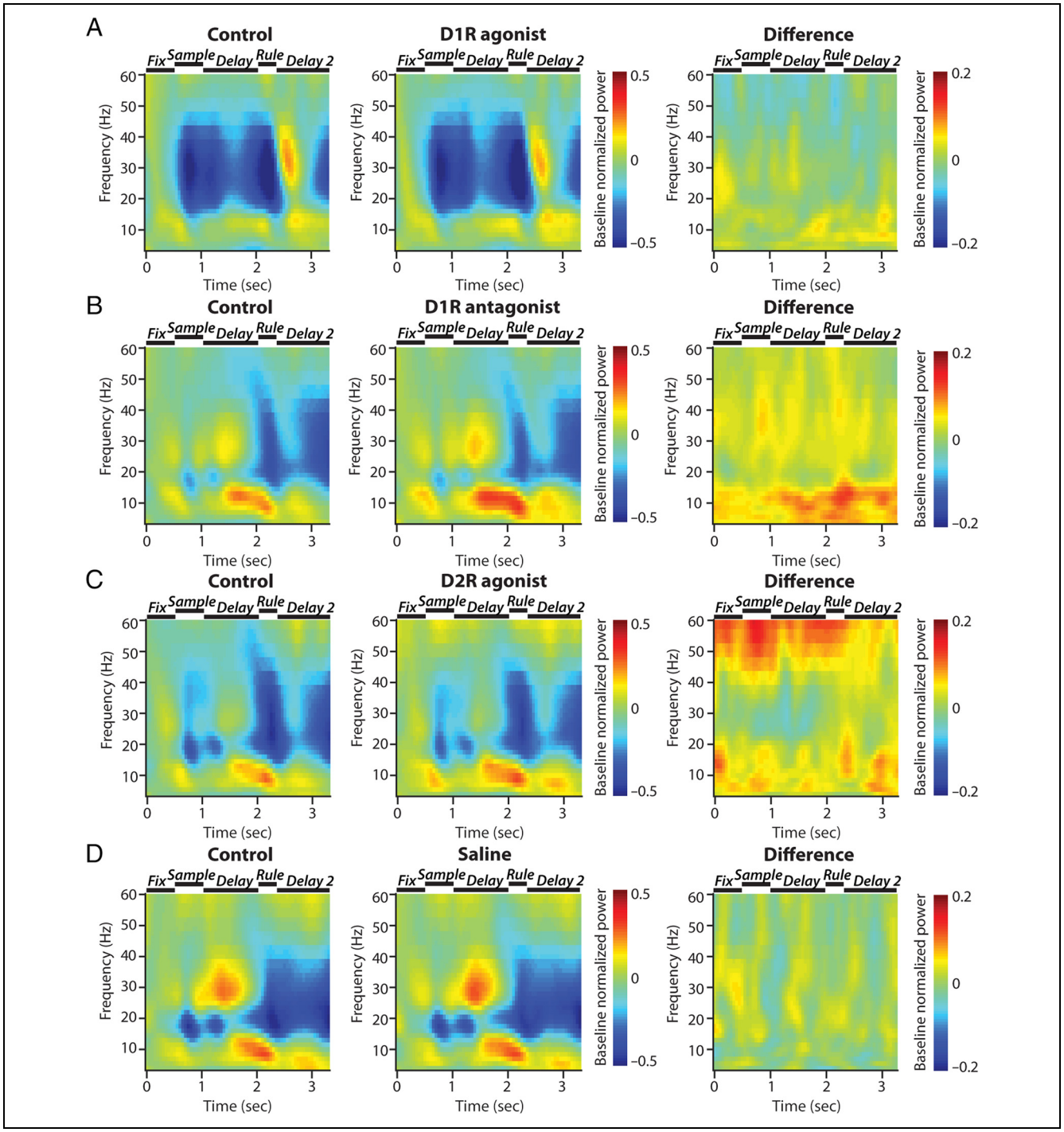

Figure 5. Time-dependent modulation of internally generated LFP power spectra. (A) Time–frequency plot with color-coded baseline-normalized LFP power for control conditions (left) and after SKF81297 application (right). Power spectra showed prominent modulation by visual stimuli (sample stimulus, 0.5 sec; rule cue, 2.0 sec) for frequencies around 10 Hz and during delay periods for higher frequencies. (B) Conventions as in A for SCH23390 showing a prominent increase in power for low frequencies around 10 Hz. (C) Conventions as in A for quinpirole showing an increase in power for higher frequencies. (D) Conventions as in A for saline controls with no modulation of LFP power.

(Figure 6C), blocking D1Rs increased power in the low-frequency theta/alpha range between 4 and 17 Hz (ΔPower = 5.0 $\pm$ 0.8 μV^2, $n = 97$, $p < .01$ in 10 consecutive frequency bands; Figure 6D). In addition, the beta/low gamma range between 27 and 32 Hz was enhanced after blocking D1Rs (ΔPower = 5.4 $\pm$ 1.9 μV^2, $n = 97$, $p < .01$ in five consecutive frequency bands; Figure 6D).

Stimulating D2Rs also enhanced power in the theta/alpha range between 6 and 16 Hz (ΔPower = 3.4 $\pm$ 0.8 μV^2, $n = 67$, $p < .01$ in 10 consecutive frequency bands) but

also increased LFP power in the high-frequency gamma range between 55 and 60 Hz (ΔPower = 2.1 ± 0.9 μV^2, n = 97, p < .01 in two consecutive frequency bands; Figure 6E).

Application of normal saline as a control did not produce changes in LFP power (Figure 6F). Thus, dopamine receptor-specific LFP power modulation during the delay period matched the frequency bands that were dependent on the task rule.

D1Rs Modulated Rule-dependent LFP Power

To assess if dopamine receptors modulated the selectivity of rule-dependent LFP power, we quantified rule-dependent LFP power by a rule modulation index for responses in the Delay 2 period. The rule modulation index was defined by the difference in LFP power of "larger than" and "less than" trials divided by the sum. We defined two frequency bands based on the frequency ranges showing a significant rule modulation of LFP power (p < .01, signed rank test, see Figure 6A): The "beta" range between 24 and 36 Hz, and the "gamma" range between 46 and 60 Hz (Figure 6A). Confirming our previous analysis, we observed a negative rule modulation index in the beta band and a positive rule modulation index in the gamma band (Figure 7A, C, E).

However, we did not find a significant modulation by either D1R or D2R targeting drugs (Figure 7A, C, E, signed rank test, p > .05 for all comparisons). To analyze rule modulation in more detail, we selected individual channels showing significant drug modulation during either beta or gamma bands (p < .05, signed rank test over trials for each channel). This analysis revealed no modulation for stimulating D1Rs (p > .05, n = 36, signed rank test; Figure 7B). However, D1R blockade resulted in a significant decrease of rule modulation indices in the beta band (ΔMI = −0.02 ± 0.008, p = .04, n = 33, signed rank test), thus increasing the strength of rule modulation, while also a decrease of rule modulation indices in the gamma band (ΔMI = −0.01 ± 0.005, p = .04, n = 33, signed rank test), thus decreasing the strength of rule modulation (Figure 7D).

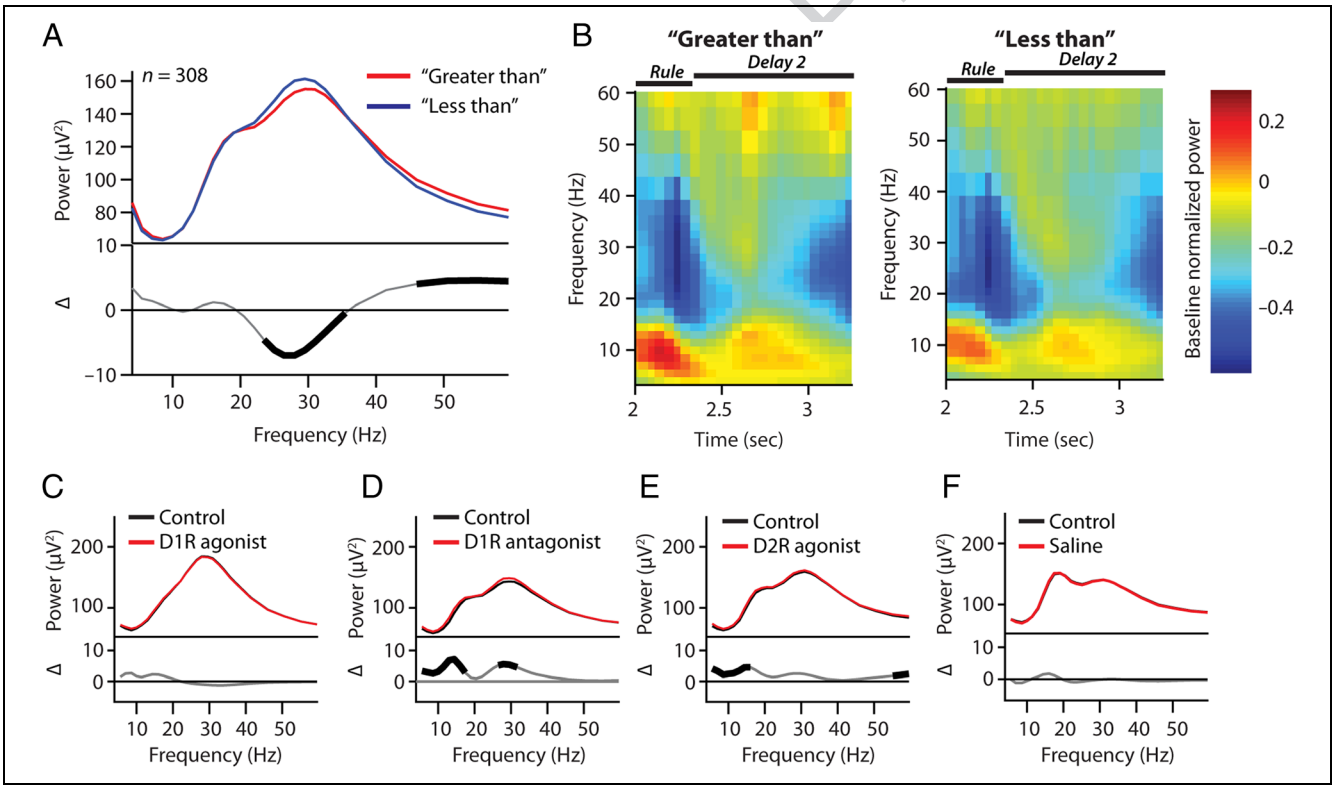

Figure 6. Numerical rules modulated internally generated LFP power spectra. (A) Trial-averaged power spectra during control conditions without drug application for "greater than" and "less than" rule trials (top). The difference between both conditions ("greater than" minus "less than," bottom) shows a suppression of LFP power between 24 and 36 Hz and an enhancement of LFP power above 46 Hz for the "greater than" rule compared with the "less than" rule (marked by thick line segments in the bottom plot). (B) Time–frequency plot with color-coded baseline-normalized LFP power compared for "greater than" and "less than" trials during the second delay period revealing similar power modulations as in (A). (C) Raw power spectra for control conditions and after applying SKF81297 during the second delay period after rule cue presentation (top). SKF8127 application did not show LFP power modulation (bottom). (D) Same conventions as in C for SCH23390 showing an increase of LFP power below 18 Hz and between 25 and 34 Hz. (E) Same conventions as in C for quinpirole, showing an increase in LFP power between 6 and 19 Hz and above 55 Hz. (F) Same conventions as in C with no effects on LFP power after application of normal saline. n, number of channels; thick lines correspond to frequencies with significant drug-induced changes in LFP power (p < .01, signed rank test).

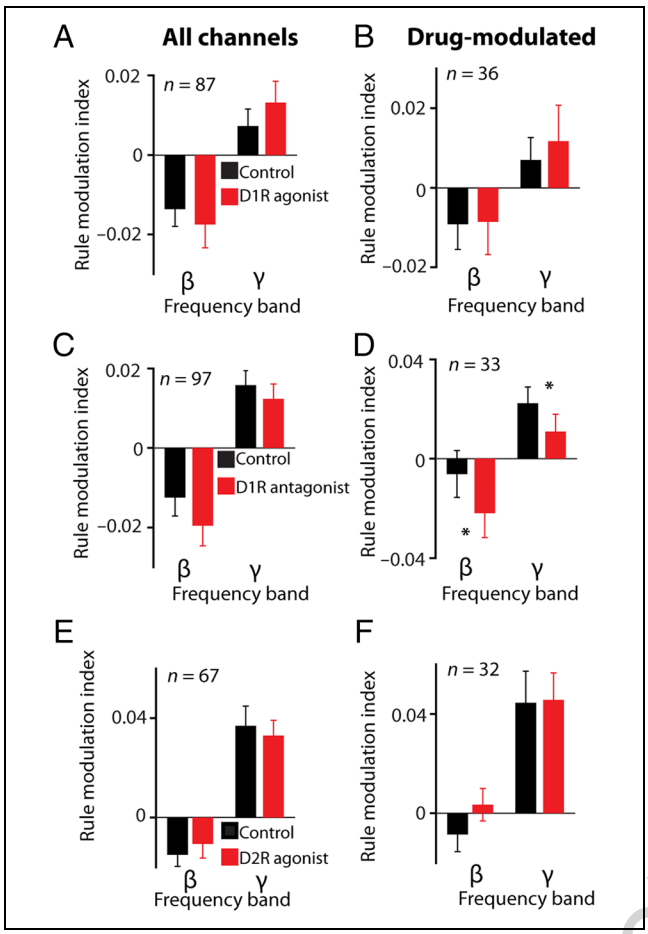

Figure 7. Dopamine receptor modulation of rule-selective LFP power. (A) Rule modulation index, defined as the difference in LFP power in the second delay period for "larger than" and "smaller than" trials for two distinct frequency bands ("beta," 24–36 Hz; "gamma," 46–60 Hz), which showed a significant modulation by rule (see Figure 6A). SKF81297 application did not show a change of rule-selective LFP power. (B) Same conventions as in (A) for SKF81297 for a subset of channels showing a significant drug-induced modulation of LFP power in the second delay period (rank sum test, $p < .05$). (C) Same conventions as in A for SCH23390. (D) Same conventions as in B for SCH23390. Note that blocking D1Rs influenced rule modulation indices. (E) Same conventions as in A for quinpirole. (F) Same conventions as in B for quinpirole.

Stimulating D2Rs had no effect on rule modulation indices ($p > .05$, $n = 36$, signed rank test; Figure 7F). Thus, blocking D1Rs modulated rule-dependent LFP power in a subset of channels.

DISCUSSION

Our findings show that modulation of dopamine receptors strongly influences neural oscillations during cognitive processing in pFC. We quantified neural oscillations using LFP power in frequency bands with clear power peaks during the baseline and while the monkeys were engaged in the numerical rule-switching task. Dopamine receptors did not modulate LFP power reflecting sensory-evoked potentials driven by external sensory cues. However, internally generated neural oscillations were prominently and differentially modulated by D1Rs and D2Rs. Although both D1Rs and D2Rs changed low-frequency theta (~4–8 Hz)/alpha (~8–15 Hz) band power, only blocking D1Rs increased power in the beta band (~15–35 Hz). Stimulating D2Rs, instead, increased power in the gamma band (~35–60 Hz). Notably, beta and gamma band power was dependent on the numerical rule the monkeys had to apply: For the "greater than" rule, beta power was lower and gamma power was higher compared with the "less than" rule. These results suggest that dopamine receptors assume dissociable roles in modulating cortical oscillations relevant for cognitive behavior.

Common Mechanism of D1Rs and D2Rs in Modulating Theta/Alpha Band Power

Blocking D1Rs or stimulating D2Rs increased the strength of low-frequency theta and alpha band oscillations. This suggests that both dopamine receptor families might modulate these frequency bands by a common mechanism: Blocking D1Rs enhances the D2R influence in a D1R/D2R balance (Seamans & Yang, 2004). Because blocking D1Rs shows similar effects as stimulating D2Rs in theta and alpha frequency bands, these results argue for an antagonistic role of D1Rs and D2Rs in modulating low-frequency oscillations.

Theta-band activity has been associated with memory and learning (Benchenane et al., 2011). For instance, theta oscillations between hippocampus and pFC are synchronized in rats learning a spatial rule, and dopamine infusion in pFC mimicked these effects (Benchenane et al., 2010). Our results suggest that increased theta oscillations in pFC after dopamine infusion is driven by an increase of D2R activation compared with D1R activation. Prefrontal theta oscillations also play a more general role in working memory. For example, pFC theta oscillations synchronize with visual areas during visual working memory in monkeys (Liebe, Hoerzer, Logothetis, & Rainer, 2012) and show sustained power increase during visual working memory in humans (Raghavachari et al., 2001). This suggests that theta activity does not only play a role in spatial cognition but has a more general role in working memory (Roux & Uhlhaas, 2014). In agreement with these findings, we observed sharp theta power increases after presentation of task-relevant visual items, suggesting that theta oscillations gate the content of working memory rather than maintaining relevant information (Raghavachari et al., 2001) essential for encoding rather than maintenance of relevant information (Spellman et al., 2015). Interestingly, a gating mechanism during working memory has also previously been proposed for dopamine (D'Ardenne et al., 2012; Cohen, Braver, & O'Reilly, 1996). Indeed, D2Rs modulate pFC network activity particularly after presentation of visual

items to be held in working memory (Ott & Nieder, 2017), possibly by increasing interneuron control over pyramidal cells (Ott & Nieder, 2017; Benchenane et al., 2010). Prefrontal theta oscillations therefore might gate task-relevant sensory items primarily through the activation of D2R over D1Rs in pFC.

The power of alpha band oscillations was also enhanced by both blocking D1Rs or activating D2Rs. Increased alpha oscillations have been associated with the suppression of task-irrelevant information (Roux & Uhlhaas, 2014). Alpha power in pFC increases with working memory demands in humans (Jensen, Gelfand, Kounios, & Lisman, 2002) and is thought to inhibit top–down visual areas (Jokisch & Jensen, 2007). In agreement with this hypothesis, Buschman, Denovellis, Diogo, Bullock, and Miller (2012) found an increase in alpha synchrony within pFC when monkeys had to suppress the selection of the behaviorally dominant task rule in favor of the behaviorally weaker rule. Blocking either D1Rs or D2Rs increased alpha power in pFC of monkeys learning cue–saccade associations and impaired learning of novel associations (Puig & Miller, 2012, 2015). Our findings are in agreement with these results. We found peak alpha oscillations after presentation of task-relevant visual cues as well as enhanced alpha power during delay periods. Alpha power was increased by either blocking D1Rs or stimulating D2Rs, suggesting that a bias toward D2R activation increases alpha oscillations in pFC. Interestingly, D2Rs have been implicated in flexibly switching between behavioral strategies (Floresco & Magyar, 2006) and modulate neuronal activity encoding task rules (Ott et al., 2014). This suggests that D2R mediated modulation of alpha power might reflect the strength of suppression of the behaviorally irrelevant task rules.

Dissociable Mechanisms of D1Rs and D2Rs in Modulating Beta/Gamma Band Power

In contrast to the common modulation of low-frequency theta/alpha power by D1Rs and D2Rs, the two receptor families differentially affected beta and gamma oscillations in pFC. Strikingly, these beta and gamma oscillations were dependent on the behavioral rule the monkeys were applying. Blocking D1Rs decreased the rule selectivity of LFP power in the gamma band while increasing the selectivity in the beta band. Thus, beta and gamma oscillations are likely modulated by dissociable receptor mechanisms.

We found that beta oscillations were suppressed during delay periods compared with baseline. Blocking D1R increased beta power, whereas D2Rs did not modulate beta oscillations. An enhancement of beta power by blocking D1Rs had also been reported in a previous study, in which blocking prefrontal D1Rs impaired learning new cue–saccade associations (Puig & Miller, 2012). Beta oscillations have been associated with top–down attentional control (Buschman & Miller, 2007) and are related to the maintenance of the current cognitive state (Benchenane et al., 2011; Engel & Fries, 2010). In monkeys that switched between a "color" rule and an "orientation" rule, synchrony of beta band oscillations within pFC was rule-dependent (Buschman et al., 2012). These results suggest that beta oscillations are important in selecting and maintaining relevant information and rules for the task at hand (Buschman et al., 2012). Beta oscillations may therefore provide a communication channel between neural ensembles. Blocking D1Rs impairs sustained single-neuron encoding of task rules (Ott et al., 2014) and working memory (Vijayraghavan et al., 2007), which is in accordance for a role of beta oscillations in maintaining relevant information in pFC. Supporting this idea, D1Rs modulate the recovery of task-relevant information in pFC from distracting stimuli (Jacob, Stalter, & Nieder, 2016). Together, these results support the hypothesis that D1R activation contributes to stabilizing prefrontal representations (Durstewitz & Seamans, 2008; Seamans & Yang, 2004) possibly via beta oscillations. However, blocking D1Rs increased the rule-selective LFP signal in the beta band. It remains to be resolved if and how neuronal and oscillatory activity in pFC is locked during the manipulation of dopamine receptors.

In contrast to beta oscillations, we found that D2Rs increased the power of gamma oscillations, whereas D1Rs did not modulate gamma oscillations. This finding is in line with previous findings, in which blocking D1Rs did not alter gamma oscillations (Puig & Miller, 2012). Gamma modulation by D2Rs has been reported in rodent studies (Kocsis et al., 2014; Andersson et al., 2012), but not in primates learning associations (Puig & Miller, 2015). Here we found that gamma band power was also rule-dependent, raising the possibility that D2Rs modulate gamma-dependent neural processing, such as bottom–up attentional mechanisms (Miller & Buschman, 2013; Benchenane et al., 2011). Gamma oscillations are synchronized during bottom–up attention between monkey cortical visual areas (Bosman et al., 2012) and between pFC and parietal areas (Buschman & Miller, 2007). Increased gamma power correlates with working memory performance in humans (Jokisch & Jensen, 2007) and increases with higher working memory load (Roux, Wibral, Mohr, Singer, & Uhlhaas, 2012). Therefore, gamma band oscillations have been suggested to underlie working memory maintenance (Roux & Uhlhaas, 2014). Consistent with this idea, neuronal rule coding in pFC is also enhanced by D2R stimulation (Ott et al., 2014), as well as working memory coding (Ott & Nieder, 2017). In addition, transitions in population activity at the beginning of memory delay periods are modulated by D2Rs, suggesting that D2Rs mediate switching between pFC representations (Ott & Nieder, 2017). The enhanced gamma band power induced by D2R stimulation may

allow for bottom–up updating of task-relevant information in pFC, supporting the hypothesis that D2Rs mediate switching of prefrontal representations.

Dopamine Receptors Modulate Internally Generated Oscillations during Cognitive Control

Interestingly, we did not find any modulation of externally driven sensory-evoked potentials by dopamine receptor manipulations. This is surprising, given the evidence that attention modulates ERPs in sensory cortices (Lakatos, Karmos, Mehta, Ulbert, & Schroeder, 2008). This modulation in sensory cortices is possibly mediated by a phase reset of ongoing neural oscillations (Lakatos et al., 2009). In pFC, however, we did not find any evidence for a dopamine-dependent change in phase coherence. This absence of a change in phase coherence could be related to our task demands and the well-established conditional association of sensory cues with rules. This is supported by the recent finding that the learning stimulus–reward association shifts LFP components from sensory-evoked potentials to internally generated oscillations (Brincat & Miller, 2016). Because dopamine receptor activation is necessary for the learning associations and modulates LFP power in pFC (Puig & Miller, 2012, 2015), dopamine might play a specific role during learning that is not captured by our study.

Together, our results emphasize that dopamine has a strong and direct influence on internally generated neural oscillations in pFC, and these effects are dissociable at the receptor level. The pattern of dopamine receptor-mediated modulation of LFP power suggests specialized roles of dopamine receptors in influencing oscillatory activity during rule processing, which likely generalize to other pFC-dependent cognitive control functions. Thus, dopamine receptor modulation of cognitive functions might be mediated by controlling internal cortical oscillations, which coordinate neural ensembles representing current task demands. Insights from clinical conditions with known disturbances in the dopamine system support this idea because they also show altered neural oscillations (Lisman, 2012), in particular of the gamma band (Gonzalez-Burgos, Cho, & Lewis, 2015). Mechanistically, gamma oscillations are thought to be driven by cortical interneurons (Furth, Mastwal, Wang, Buonanno, & Vullhorst, 2013; Sohal et al., 2009). Interneurons seem to be the main target of D2R modulation of prefrontal networks (Ott & Nieder, 2017). Thus, increased activation of D2Rs in pFC might lead to disturbed gamma band oscillations and executive functions. It remains to be resolved if changes in prefrontal dopamine signaling directly disturbs the interaction through synchronization with other areas during cognitive control. So far, emerging evidence suggests a strong role for dopamine in controlling executive control in pFC at different modes of information processing through dissociable actions of dopamine receptors.

Acknowledgments

This work was supported by grants from the German Research Foundation (DFG) to A. N. (618/4-1 and NI 618/5-1). T. O. designed and performed experiments, analyzed data, and wrote the paper; S. W. analyzed data and wrote the paper; A. N. designed experiments and wrote the paper.

Reprint requests should be sent to Andreas Nieder, University of Tuebingen, Auf der Morgenstelle 28, 72076 Tuebingen, Germany, or via e-mail: andreas.nieder@uni-tuebingen.de.

REFERENCES

Andersson, R., Johnston, A., & Fisahn, A. (2012). Dopamine D4 receptor activation increases hippocampal gamma oscillations by enhancing synchronization of fast-spiking interneurons. *PLoS One, 7,* e40906.

Benchenane, K., Peyrache, A., Khamassi, M., Tierney, P. L., Gioanni, Y., Battaglia, F. P., et al. (2010). Coherent theta oscillations and reorganization of spike timing in the hippocampal-prefrontal network upon learning. *Neuron, 66,* 921–936.

Benchenane, K., Tiesinga, P. H., & Battaglia, F. P. (2011). Oscillations in the prefrontal cortex: A gateway to memory and attention. *Current Opinion in Neurobiology, 21,* 475–485.

Bongard, S., & Nieder, A. (2010). Basic mathematical rules are encoded by primate prefrontal cortex neurons. *Proceedings of the National Academy of Sciences, U.S.A., 107,* 2277–2282.

Bosman, C. A., Schoffelen, J.-M., Brunet, N., Oostenveld, R., Bastos, A. M., Womelsdorf, T., et al. (2012). Attentional stimulus selection through selective synchronization between monkey visual areas. *Neuron, 75,* 875–888.

Brincat, S. L., & Miller, E. K. (2016). Prefrontal cortex networks shift from external to internal modes during learning. *Journal of Neuroscience, 36,* 9739–9754.

Brozoski, T. J., Brown, R. M., Rosvold, H. E., & Goldman, P. S. (1979). Cognitive deficit caused by regional depletion of dopamine in prefrontal cortex of rhesus monkey. *Science, 205,* 929–932.

Buschman, T. J., Denovellis, E. L., Diogo, C., Bullock, D., & Miller, E. K. (2012). Synchronous oscillatory neural ensembles for rules in the prefrontal cortex. *Neuron, 76,* 838–846.

Buschman, T. J., & Miller, E. K. (2007). Top–down versus bottom–up control of attention in the prefrontal and posterior parietal cortices. *Science, 315,* 1860–1862.

Cohen, J. D., Braver, T. S., & O'Reilly, R. C. (1996). A computational approach to prefrontal cortex, cognitive control and schizophrenia: Recent developments and current challenges. *Philosophical Transactions of the Royal Society B: Biological Sciences, 351,* 1515–1527.

D'Ardenne, K., Eshel, N., Luka, J., Lenartowicz, A., Nystrom, L. E., Cohen, J. D., et al. (2012). Role of prefrontal cortex and the midbrain dopamine system in working memory updating. *Proceedings of the National Academy of Sciences, U.S.A., 109,* 19900–19909.

Durstewitz, D., & Seamans, J. K. (2008). The dual-state theory of prefrontal cortex dopamine function with relevance to catechol-o-methyltransferase genotypes and schizophrenia. *Biological Psychiatry, 64,* 739–749.

Eiselt, A.-K., & Nieder, A. (2013). Representation of abstract quantitative rules applied to spatial and numerical magnitudes in primate prefrontal cortex. *Journal of Neuroscience, 33,* 7526–7534.

Engel, A. K., & Fries, P. (2010). Beta-band oscillations—Signalling the status quo? *Current Opinion in Neurobiology, 20,* 156–165.

Floresco, S. B., & Magyar, O. (2006). Mesocortical dopamine modulation of executive functions: Beyond working memory. *Psychopharmacology, 188,* 567–585.
Floresco, S. B., Magyar, O., Ghods-Sharifi, S., Vexelman, C., & Tse, M. T. L. (2006). Multiple dopamine receptor subtypes in the medial prefrontal cortex of the rat regulate set-shifting. *Neuropsychopharmacology, 31,* 297–309.
Furth, K. E., Mastwal, S., Wang, K. H., Buonanno, A., & Vullhorst, D. (2013). Dopamine, cognitive function, and gamma oscillations: Role of D4 receptors. *Frontiers in Cellular Neuroscience, 7,* 102.
Gonzalez-Burgos, G., Cho, R. Y., & Lewis, D. A. (2015). Alterations in cortical network oscillations and parvalbumin neurons in schizophrenia. *Biological Psychiatry, 77,* 1031–1040.
Jacob, S. N., Ott, T., & Nieder, A. (2013). Dopamine regulates two classes of primate prefrontal neurons that represent sensory signals. *Journal of Neuroscience, 33,* 13724–13734.
Jacob, S. N., Stalter, M., & Nieder, A. (2016). Cell-type-specific modulation of targets and distractors by dopamine D1 receptors in primate prefrontal cortex. *Nature Communications, 7,* 13218.
Jensen, O., Gelfand, J., Kounios, J., & Lisman, J. E. (2002). Oscillations in the alpha band (9–12 Hz) increase with memory load during retention in a short-term memory task. *Cerebral Cortex, 12,* 877–882.
Jokisch, D., & Jensen, O. (2007). Modulation of gamma and alpha activity during a working memory task engaging the dorsal or ventral stream. *Journal of Neuroscience, 27,* 3244–3251.
Kocsis, B., Lee, P., & Deth, R. (2014). Enhancement of gamma activity after selective activation of dopamine D4 receptors in freely moving rats and in a neurodevelopmental model of schizophrenia. *Brain Structure & Function, 219,* 2173–2180.
Lakatos, P., Karmos, G., Mehta, A. D., Ulbert, I., & Schroeder, C. E. (2008). Entrainment of neuronal attentional selection. *Science, 320,* 23–25.
Lakatos, P., O'Connell, M. N., Barczak, A., Mills, A., Javitt, D. C., & Schroeder, C. E. (2009). The leading sense: Supramodal control of neurophysiological context by attention. *Neuron, 64,* 419–430.
Liebe, S., Hoerzer, G. M., Logothetis, N. K., & Rainer, G. (2012). Theta coupling between V4 and prefrontal cortex predicts visual short-term memory performance. *Nature Neuroscience, 15,* 456–462.
Lisman, J. (2012). Excitation, inhibition, local oscillations, or large-scale loops: What causes the symptoms of schizophrenia? *Current Opinion in Neurobiology, 22,* 537–544.
Lopes da Silva, F. (2013). EEG and MEG: Relevance to neuroscience. *Neuron, 80,* 1112–1128.
Miller, E. K., & Buschman, T. J. (2013). Cortical circuits for the control of attention. *Current Opinion in Neurobiology, 23,* 216–222.
Miller, E. K., & Cohen, J. D. (2001). An integrative theory of prefrontal cortex function. *Annual Review of Neuroscience, 24,* 167–202.
Nieder, A. (2016). The neuronal code for number. *Nature Reviews Neuroscience, 17,* 366–382.
Nieder, A., & Miller, E. K. (2003). Coding of cognitive magnitude: Compressed scaling of numerical information in the primate prefrontal cortex. *Neuron, 37,* 149–157.
Ott, T., Jacob, S. N., & Nieder, A. (2014). Dopamine receptors differentially enhance rule coding in primate prefrontal cortex neurons. *Neuron, 84,* 1317–1328.
Ott, T., & Nieder, A. (2017). Dopamine D2 receptors enhance population dynamics in primate prefrontal working memory circuits. *Cerebral Cortex, 27,* 4423–4435.
Parker, K. L., Chen, K.-H., Kingyon, J. R., Cavanagh, J. F., & Narayanan, N. S. (2014). D1-dependent 4 Hz oscillations and ramping activity in rodent medial frontal cortex during interval timing. *Journal of Neuroscience, 34,* 16774–16783.
Parker, K. L., Ruggiero, R. N., & Narayanan, N. S. (2015). Infusion of D1 dopamine receptor agonist into medial frontal cortex disrupts neural correlates of interval timing. *Frontiers in Behavioral Neuroscience, 9,* 1–7.
Puig, M. V., & Miller, E. K. (2012). The role of prefrontal dopamine D1 receptors in the neural mechanisms of associative learning. *Neuron, 74,* 874–886.
Puig, M. V., & Miller, E. K. (2015). Neural substrates of dopamine D2 receptor modulated executive functions in the monkey prefrontal cortex. *Cerebral Cortex, 25,* 2980–2987.
Puig, M. V., Rose, J., Schmidt, R., & Freund, N. (2014). Dopamine modulation of learning and memory in the prefrontal cortex: Insights from studies in primates, rodents, and birds. *Front Neural Circuits, 8,* 93.
Raghavachari, S., Kahana, M. J., Rizzuto, D. S., Caplan, J. B., Kirschen, M. P., Bourgeois, B., et al. (2001). Gating of human theta oscillations by a working memory task. *Journal of Neuroscience, 21,* 3175–3183.
Ray, S., & Maunsell, J. H. R. (2011). Different origins of gamma rhythm and high-gamma activity in macaque visual cortex. *PLoS Biol, 9,* e1000610.
Robbins, T. W., & Arnsten, A. F. T. (2009). The neuropsychopharmacology of fronto-executive function: Monoaminergic modulation. *Annual Review of Neuroscience, 32,* 267–287.
Roux, F., & Uhlhaas, P. J. (2014). Working memory and neural oscillations: Alpha–gamma versus theta–gamma codes for distinct WM information? *Trends in Cognitive Sciences, 18,* 16–25.
Roux, F., Wibral, M., Mohr, H. M., Singer, W., & Uhlhaas, P. J. (2012). Gamma-band activity in human prefrontal cortex codes for the number of relevant items maintained in working memory. *Journal of Neuroscience, 32,* 12411–12420.
Sauseng, P., Klimesch, W., Gruber, W. R., Hanslmayr, S., Freunberger, R., & Doppelmayr, M. (2007). Are event-related potential components generated by phase resetting of brain oscillations? A critical discussion. *Neuroscience, 146,* 1435–1444.
Seamans, J. K., & Yang, C. R. (2004). The principal features and mechanisms of dopamine modulation in the prefrontal cortex. *Progress in Neurobiology, 74,* 1–58.
Siegel, M., Donner, T. H., Oostenveld, R., Fries, P., & Engel, A. K. (2008). Neuronal synchronization along the dorsal visual pathway reflects the focus of spatial attention. *Neuron, 60,* 709–719.
Singer, W. (2009). Distributed processing and temporal codes in neuronal networks. *Cognitive Neurodynamics, 3,* 189–196.
Sohal, V. S., Zhang, F., Yizhar, O., & Deisseroth, K. (2009). Parvalbumin neurons and gamma rhythms enhance cortical circuit performance. *Nature, 459,* 698–702.
Spellman, T., Rigotti, M., Ahmari, S. E., Fusi, S., Gogos, J. A., & Gordon, J. A. (2015). Hippocampal–prefrontal input supports spatial encoding in working memory. *Nature, 522,* 309–314.
Stoet, G., & Snyder, L. H. (2009). Neural correlates of executive control functions in the monkey. *Trends in Cognitive Sciences, 13,* 228–234.
Thiele, A., Delicato, L. S., Roberts, M. J., & Gieselmann, M. A. (2006). A novel electrode–pipette design for simultaneous recording of extracellular spikes and iontophoretic drug

application in awake behaving monkeys. *Journal of Neuroscience Methods, 158,* 207–211.
Uhlhaas, P., Gordon, P., Lima, B., Melloni, L., Neuenschwader, S., Nikolic, D., et al. (2009). Neural synchrony in cortical networks: History, concept and current status. *Frontiers in Integrative Neuroscience, 3,* 1–19.
Vijayraghavan, S., Wang, M., Birnbaum, S. G., Williams, G. V., & Arnsten, A. F. T. (2007). Inverted-U dopamine D1 receptor actions on prefrontal neurons engaged in working memory. *Nature Neuroscience, 10,* 376–384.
Wang, M., Vijayraghavan, S., & Goldman-Rakic, P. S. (2004). Selective D2 receptor actions on the functional circuitry of working memory. *Science, 303,* 853–856.
Womelsdorf, T., & Fries, P. (2007). The role of neuronal synchronization in selective attention. *Current Opinion in Neurobiology, 17,* 154–160.